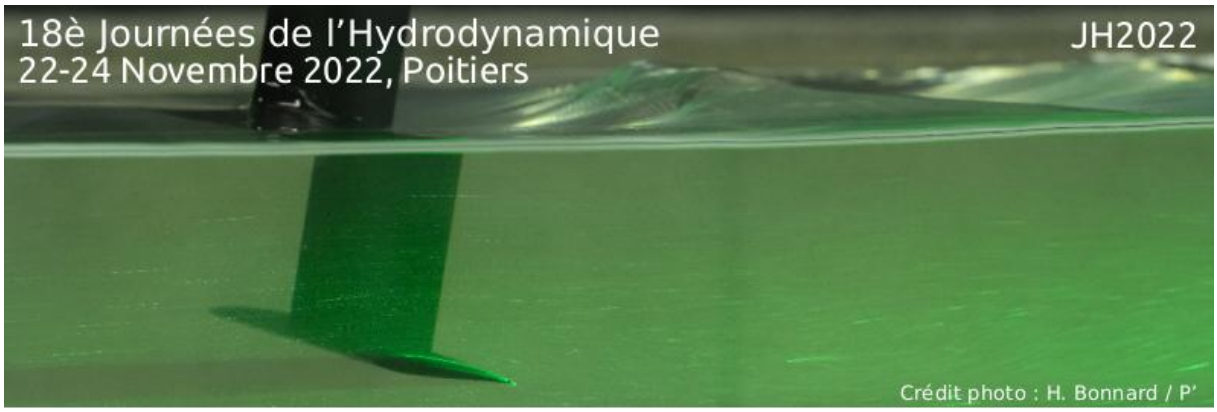

COMPUTATION OF SECOND-ORDER WAVE LOADS ON FLOATING OFFSHORE WIND TURBINE PLATFORMS IN BI-CHROMATIC BI-DIRECTIONAL WAVES USING OPEN-SOURCE POTENTIAL FLOW SOLVER NEMOH

R. KURNIA, G. DUCROZET

ruddy.kurnia@ec-nantes.fr; guillaume.ducrozet@ec-nantes.fr

Nantes Université, Ecole Centrale Nantes, CNRS, LHEEA, UMR 6598, F-44000 Nantes, France

Summary

Second-order wave loads on a floating structure may excite resonance phenomena, such as slow-drift or springing, at the natural frequencies of the floating structure. Therefore, taking into account the response of a floating offshore wind turbine (FOWT) platform under non-linear wave loads is of paramount importance for its design. This paper presents computation results of the quadratic transfer functions (QTFs) for sum- and difference-frequencies wave loads on FOWT platforms using open-source potential flow, boundary element solver NEMOH. The QTFs are composed of quadratic terms and second-order potential terms. The quadratic terms are computed based on the near-field formulation, while the computation of potential terms is based on the indirect method that uses the Green-formulation and an assisting function, which is the normalized radiation potential. In this paper, we show the NEMOH QTFs computation on two FOWT platforms, the OC4-DeepCwind submersible platform and the SOFTWIND spar-type platform. The results are compared with the reference commercial software HYDROSTAR. Excellent agreement between the two QTFs results is achieved. The focus is put on bi-directional difference-frequency of surge, heave, and pitch QTFs and on sum-frequency full QTFs.

I – Introduction

NEMOH [1]is the first open-source potential flow boundary element solver that is developed at Ecole Centrale de Nantes [1]. The software is widely used for ocean engineering applications and particularly in wave-energy community [8, 12, 13]. Nowadays, offshore wind energy has huge potential to be a key element in the energy transition to come. In this aspect, potential flow codes, such as NEMOH, could an role in the hydrodynamic design of floating offshore wind turbines.

In the design of a FOWT, nonlinear wave-structure interactions have to be taken into account to prevent uncontrolled motions of the floating structure due to large excitation loads at the resonance frequencies of the structure with the presence of mooring (i.e low-frequency loads). In this aspect, the EU-funded project FLOATECH [2]contributes the development of the open-source QBlade-Ocean software. In QBlade-Ocean, the coupling of three open-source softwares are developed. QBlade software [14], dedicated to the design of FOWT that is developed at TU-Berlin, requires hydrodynamics wave-input. NEMOH contributes as an external source for the first- and second-order hydrodyamics input and HOS-Ocean [6] for the nonlinear wave input.

This paper reports development and verification of the second-order module in NEMOH particularly for bi-directional quadratic transfer functions (QTFs). The first development of the module has been reported in [9]. Extensive verification of recent development of the QTF module for uni-directional QTFs has been reported in [10].

The second-order wave loads are composed of the quadratic part and the potential part. The quadratic part are based on the near-field method as described in [3]. The potential part is based on the indirect method [3, 7] that uses the Green-formulation and an assisting function, that is the normalized radiation potential. Then, the potential part requires an integration of the second-order body forcing terms over the body hull and integration of the second-order free-surface forcing terms over semi-infinite radius.

The organisation of the paper is as follows. Section II describes the notation used in this paper. Section III and IV describe the second-order wave loads formulations used and implemented in NEMOH. In Section V, NEMOH full QTF implementation is verified through the comparison to HYDROSTAR commercial software [2]. Two floating offshore wind turbine platforms are tested : the spar-buoy type SOFTWIND platform [5] and the OC4-semisubmersible platform [11]. Conclusion is given in Section VI.

II – Notation

We start with notation and definition that are used in this paper. The floating body is defined with 6 degrees of freedom determined at center of gravity (CoG), $\boldsymbol{\xi} = (\boldsymbol{X}, \boldsymbol{\theta})$ where the positions, $\boldsymbol{X} = (X, Y, Z)$ and the orientations, $\boldsymbol{\theta} = (\theta_1, \theta_2, \theta_3)$. The displacement of points at the hull are specified by a body of vector $\boldsymbol{r}$ with respect to the CoG as $\boldsymbol{\mathcal{X}} = \boldsymbol{X} + R(\boldsymbol{r})$ and R is a rotation operator, $R(\boldsymbol{r}) = \boldsymbol{\theta} \times \boldsymbol{r}$. The six-dimensional generalized normal vector is defined as $\boldsymbol{\nu} = (\boldsymbol{n}, \boldsymbol{r} \times \boldsymbol{n})^T$ with the unit normal vector, $\boldsymbol{n}$, towards the fluid domain and the normal vectors at the mean body positions as $\boldsymbol{\nu}_0$ and $\boldsymbol{n}_0 = (n_{0_1}, n_{0_2}, n_{0_3})$. The fluid-potential is denoted $\Phi(\boldsymbol{x}, t)$, in the cartesian coordinate $\vec{x} = (x, y)$, $\boldsymbol{x} = (\vec{x}, z)$ for time t, the fluid velocity, $\nabla\Phi$, and the time derivative of the potential, $\partial_t\Phi$.

1. https://lheea.ec-nantes.fr/valorisation/logiciels-et-brevets/nemoh-presentation
2. https://www.floatech-project.com/

III – Second-Order Hydrodynamics Forces

This section describes formulation of the second-order hydrodynamic force in NEMOH for bi-directional bi-chromatic waves.

In the potential flow problem of wave-structure interaction, fluid is assumed to be inviscid and the flow is irrotational. Fluid is also considered incompressible so that the fluid-potential in the interior domain is described by Laplace equation. Following boundary conditions have to be considered ; the free-surface conditions, the diffraction and radiation conditions on the body hull, the impermeable bottom condition and the radiation wave condition at the far field.

The potential flow problem can be truncated for the first-order and the second-order problems by applying a perturbation series, as shown in [3, 10]. In NEMOH, the first-order diffraction and radiation problems are solved using the three-dimensional boundary element method with the source distribution formulation. The second-order diffraction problem is not solved directly but an extended module in NEMOH allows computation of the second-order force based on the first-order diffraction and radiation solutions.

The formulation starts with the perturbation series up to and including second-order terms, (ϵ^2), of the body displacement, $\boldsymbol{\chi}$, the fluid-potential, Φ, the hydrodynamic pressure, P_H, and then the hydrodynamic force, $\boldsymbol{F}_H$.

The first-order hydrodynamic pressure, $P_H^{(1)}$, and the second-order hydrodynamic pressure, $P_H^{(2)}$, are then expressed as, with ρ is the fluid density,

$$P_H^{(1)} = -\rho\partial_t\Phi^{(1)},\; P_H^{(2)} = -\rho\left[\partial_t\Phi^{(2)} + \frac{1}{2}|\nabla\Phi^{(1)}|^2 + \boldsymbol{\chi}^{(1)}\cdot\partial_t\nabla\Phi^{(1)}\right]. \tag{1}$$

where the total potential is the sum of the incident potential and the perturbed potential, $\Phi^{(1,2)} = \Phi_I^{(1,2)} + \Phi_P^{(1,2)}$ in which the perturbed potential is sum of the diffraction and radiation potentials $\Phi_P^{(1,2)} = \Phi_D^{(1,2)} + \Phi_R^{(1,2)}$, where the radiation potential is dot product of the body velocity and the normalized radiation potential $\Phi_R^{(1,2)} = \partial_t\boldsymbol{\xi}^{(1,2)}\cdot\boldsymbol{\psi}$.

The hydrodynamic force is obtained by integrating the hydrodynamic pressure, Eq. (1), over the body hull, S_B that is composed of the integration over the mean wetted body surface, S_{B_0}, and of the integration over the perturbed body surface, ϵS. The potential over the body hull is expressed in the potential at the mean body hull position by using Taylor expansion. The hydrodynamic force is then expressed as

$$\begin{aligned}
\boldsymbol{F}_H &= -\iint_{S_{B_0}\cup\epsilon S} P_H\boldsymbol{\nu}dS = \boldsymbol{F}_H^{(1)} + \boldsymbol{F}_H^{(2)},\\
\boldsymbol{F}_H^{(1)} &= -\iint_{S_{B0}} P_H^{(1)}\boldsymbol{\nu}_0 dS, \qquad \boldsymbol{F}_H^{(2)} = R^{(1)}\left(\boldsymbol{F}_H^{(1)}\right) - \iint_{S_{B_0}} P_H^{(2)}\boldsymbol{\nu}_0 dS - \iint_{\epsilon S} P_H^{(1)}\boldsymbol{\nu}_0 dS.
\end{aligned} \tag{2}$$

The second-order hydrodynamic force is composed with sum of the quadratic terms of the first order quantities, $\boldsymbol{F}_{H_1}^{(2)}$, and the second-order potential terms, $\boldsymbol{F}_{H_2}^{(2)}$, $\boldsymbol{F}_H^{(2)} = \boldsymbol{F}_{H_1}^{(2)} + \boldsymbol{F}_{H_2}^{(2)}$.

Similarly, the second-order excitation force is composed of the quadratic terms and the potential terms. The quadratic terms of the excitation force are then obtain by adding the quadratic terms of the hydrodynamic forces, Eq. (2), with the quadratic terms of the hydrostatic forces. That leads to a term with the rotation operator applied to the inertia force, $\boldsymbol{F}_I^{(1)}$ and a term with the integral over mean waterline Γ_0 of the quadratic difference between the free-surface elevation, $\eta^{(1)} = -\frac{\partial_t\Phi^{(1)}}{g}$, and the instantaneous waterline, $\zeta_{wl}^{(1)} =$

$\mathcal{X}^{(1)}_{3_{wl}}$. The force is explicitly expressed as, with g is a gravity constant,

$$\begin{aligned}\boldsymbol{F}^{(2)}_{exc_1} =& R^{(1)}\left(\boldsymbol{F}^{(1)}_I\right) - \frac{\rho g}{2}\int_{\Gamma_0}\left[\eta^{(1)} - \zeta^{(1)}_{wl}\right]^2 \boldsymbol{\nu}_0\, d\Gamma \\ &+ \iint_{S_{B_0}} \rho\left[\frac{1}{2}|\nabla\Phi^{(1)}|^2 + \boldsymbol{\mathcal{X}}^{(1)}\cdot\partial_t\nabla\Phi^{(1)}\right]\boldsymbol{\nu}_0 dS.\end{aligned} \tag{3}$$

As in the first-order fluid potential, the second-order fluid potential is composed by the second-order incoming potential, the second-order diffraction potential and the second-order radiation potential. Separating the radiation force due to the second-order body motion, then the potential term of the second-order excitation term, $\boldsymbol{F}^{(2)}_{exc_2}$, is obtained by summing the second-order Froude-Krylov force, $\boldsymbol{F}^{(2)}_{H_I}$, and the second-order diffraction force, $\boldsymbol{F}^{(2)}_{H_D}$,

$$\boldsymbol{F}^{(2)}_{exc_2} = \boldsymbol{F}^{(2)}_{H_I} + \boldsymbol{F}^{(2)}_{H_D} \tag{4}$$

The second-order potential is assumed to be an harmonic function, which frequency is the sum- or difference-frequencies modes, $\omega^{\pm} = \omega_1 \pm \omega_2$. As the result, the second-order Froude-Krylov force and the diffraction force are also harmonic functions, and given as

$$\boldsymbol{F}^{(2)\pm}_{H_I} = -\, i\omega^{\pm}\rho\iint_{S_{B_0}} \Phi^{(2)\pm}_I \boldsymbol{\nu}_0 dS, \tag{5}$$

$$\boldsymbol{F}^{(2)\pm}_{H_D} = -\, i\omega^{\pm}\rho\iint_{S_{B_0}} \Phi^{(2)\pm}_D \boldsymbol{\nu}_0 dS. \tag{6}$$

Following [3, 7], the second-order diffraction force is obtained with the indirect method using the Green formulation with an assisting function, the normalized radiation potential, $\boldsymbol{\psi}$. Then the force, Eq. (6), is composed by the integration over the body hull of the normal derivative of the second-order incident potential and the body forcing term, $Q^{(2)\pm}_B$, and the integral over the free-surface of the diffraction free-surface forcing term, $Q^{(2)\pm}_{FD}$, leads to

$$\boldsymbol{F}^{(2)\pm}_{H_D} = i\omega^{\pm}\rho\left[\iint_{S_{B_0}}\left(\partial_{\boldsymbol{n}}\Phi^{(2)\pm}_I - Q^{(2)\pm}_B\right)\boldsymbol{\psi}^{\pm} dS + \frac{1}{g}\iint_{S_F} Q^{(2)\pm}_{FD}\,\boldsymbol{\psi}^{\pm} dS\right] \tag{7}$$

The body forcing term and the free-surface forcing term are defined in the second-order potential flow problem, as in [10], and will be given explicitly in the next section.

IV – Sum- and Difference- frequencies Excitation Forces

This section describes explicitly the expression of the sum- and difference-frequencies of the excitation forces composed by the Froude-Krylov force, the quadratic part and the potential part of the force.

IV – 1 Froude-Krylov force

Bi-chromatic, bi-directional wave propagation above constant bottom, D, with two radial frequencies ω_j, with $j = 1$ and 2, wave number vectors $\vec{k_j} = (k_j\cos\beta_j, k_j\sin\beta_j)$,

β_j is the angle from the positive x-axis and the wave number k is related with ω in the dispersion relation, $\omega = \Omega(k, D) = \sqrt{gk \tanh kD}$, described by the Airy potential as

$$\begin{aligned} \Phi_I(\boldsymbol{x}, t) =& Re\left\{\Phi_{I_1}(\boldsymbol{x})e^{-i\omega_1 t} + \Phi_{I_2}(\boldsymbol{x})e^{-i\omega_2 t}\right\} \\ \Phi_{I_j}(\boldsymbol{x}) =& -i\frac{a_j g}{\omega}\mathcal{Z}(k_j, D, z)e^{i\vec{k_j}\cdot\vec{x}} \end{aligned} \tag{8}$$

where the Airy profile $\mathcal{Z}(k, D, z) = \frac{\cosh(k(D+z))}{\cosh kD}$.

The difference- and sum- frequencies incident potentials are then obtained by applying the product identity of two bi-chromatic functions involving the Airy potential, Eq. (8), in the evaluation of the free surface forcing terms [10]. The incident potentials are then expressed, with $\omega^{\pm} = \omega_1 \pm \omega_2$, $\vec{\kappa}^{\pm} = \vec{k}_1 \pm \vec{k}_2$, $|\vec{\kappa}^{\pm}| = \sqrt{k_1^2 + k_2^2 \pm 2k_1k_2\cos(\beta_1 - \beta_2)}$, $\nu_j = \frac{\Omega^2(k_j,D)}{g}$ and the complex conjugate operator applied to a complex variable, i.e. γ as $\gamma^{\mathcal{C}_-} = \gamma^*$ and $\gamma^{\mathcal{C}_+} = \gamma$, as

$$\Phi_I^{(2)\pm}(\boldsymbol{x}, t) = Re\left\{\Phi_{I_1}^{(2)\pm}(\boldsymbol{x})e^{-i\omega^{\pm}t}\right\} \tag{9}$$

$$\Phi_{I_1}^{(2)\pm}(\boldsymbol{x}) = \frac{ia_1a_2^{\mathcal{C}_\pm}g^2e^{i\vec{\kappa}^{\pm}\cdot\vec{x}}\mathcal{Z}(|\vec{\kappa}^{\pm}|, D, z)}{-(\omega^{\pm})^2 + \Omega^2(|\vec{\kappa}^{\pm}|, D)}\left[\frac{\omega^{\pm}}{\omega_1\omega_2}\left(\vec{k}_1\cdot\vec{k}_2 \mp \nu_1\nu_2\right) + \frac{1}{2}\left[\frac{k_1^2 - \nu_1^2}{\omega_1} \pm \frac{k_2^2 - \nu_2^2}{\omega_2}\right]\right].$$

The sum- and difference-frequencies Froude Krylov force, Eq. (5), can be computed directly with the incoming potential given in Eq. (9).

IV – 2 Quadratic part

The quadratic part of the sum- and difference-frequencies excitation forces, with the quadratic transfer functions (QTFs), $\boldsymbol{T}_{F_Q}(\beta_1, \beta_2, \omega_1, \omega_2)$, is given as follows

$$\begin{aligned} \boldsymbol{F}_{exc_1}^{(2)} =& Re\left\{\boldsymbol{T}_{F_Q}^{-}a_1a_2^*e^{-i(\omega_1-\omega_2)t}\right\} + Re\left\{\boldsymbol{T}_{F_Q}^{+}a_1a_2e^{-i(\omega_1+\omega_2)t}\right\}, \\ \boldsymbol{T}_{F_Q}^{\pm} =& \left[\boldsymbol{F}_{11}^{\pm} + \boldsymbol{F}_{12}^{\pm} + \boldsymbol{F}_{13}^{\pm} + \boldsymbol{F}_{14}^{\pm}\right]/a_1a_2^{\mathcal{C}_\pm} \end{aligned} \tag{10}$$

where $\boldsymbol{F}_{11}^{\pm}$, $\boldsymbol{F}_{12}^{\pm}$, $\boldsymbol{F}_{13}^{\pm}$ and $\boldsymbol{F}_{14}^{\pm}$ are obtained from Eq. (3) by applying products of the bichromatic functions, as follows

$$\begin{aligned} \boldsymbol{F}_{11}^{\pm} =& -\frac{\rho g}{2}\int_{\Gamma_0}\left[\eta_1^{(1)} - \zeta_{wl_1}^{(1)}\right]\left[\eta_2^{(1)} - \zeta_{wl_2}^{(1)}\right]^{\mathcal{C}_\pm}\boldsymbol{\nu}_0\, d\Gamma \\ \boldsymbol{F}_{12}^{\pm} =& \frac{\rho}{2}\iint_{S_{B_0}}\left[\nabla\Phi_1^{(1)}\cdot\nabla\Phi_2^{(1)\mathcal{C}_\pm}\right]\boldsymbol{\nu}_0 dS \\ \boldsymbol{F}_{13}^{\pm} =& \frac{\rho}{2}\iint_{S_{B_0}}\left[\boldsymbol{\mathcal{X}}_1^{(1)}\cdot\left(-i\omega_2\nabla\Phi_2^{(1)}\right)^{\mathcal{C}_\pm} - \boldsymbol{\mathcal{X}}_2^{(1)\mathcal{C}_\pm}\cdot i\omega_1\nabla\Phi_1^{(1)}\right]\boldsymbol{\nu}_0 dS \\ \boldsymbol{F}_{14}^{\pm} =& \frac{1}{2}\left[R_1^{(1)}\left(\boldsymbol{F}_{I_2}^{(1)\mathcal{C}_\pm}\right) + R_2^{(1)\mathcal{C}_\pm}\left(\boldsymbol{F}_{I_1}^{(1)}\right)\right]. \end{aligned} \tag{11}$$

IV – 3 Potential part

The potential part of the difference- and sum-frequencies excitation forces, with the 6−DOF quadratic transfer function (QTF), $\boldsymbol{T}_{F_P}(\beta_1, \beta_2, \omega_1, \omega_2)$, is given as follow

$$\begin{aligned} \boldsymbol{F}_{exc_2}^{(2)} =& Re\left\{\boldsymbol{T}_{F_P}^{-}a_1a_2^*e^{-i(\omega_1-\omega_2)t}\right\} + Re\left\{\boldsymbol{T}_{F_P}^{+}a_1a_2e^{-i(\omega_1+\omega_2)t}\right\}, \\ \boldsymbol{T}_{F_P}^{\pm} =& \left[\boldsymbol{F}_{H_{I_1}}^{\pm} + \boldsymbol{F}_{H_{DB_1}}^{\pm} + \boldsymbol{F}_{H_{DF_1}}^{\pm} + \boldsymbol{F}_{H_{DF_2}}^{\pm}\right]/a_1a_2^{\mathcal{C}_\pm}, \end{aligned} \tag{12}$$

where $\boldsymbol{F}^{\pm}_{H_{I_1}}$ is the Froude-Krylov force is computed as in Eq. (5) with the incident potential in Eq. (9). The diffraction force, Eq. (7), is composed of several terms : the body forcing term, $\boldsymbol{F}^{\pm}_{H_{DB_1}}$, the free surface forcing term in the finite domain, $\boldsymbol{F}^{\pm}_{H_{DF_1}}$, and the asymptotic free surface forcing term in the infinite domain, $\boldsymbol{F}^{\pm}_{H_{DF_2}}$.

The diffraction force due to the body forcing terms is composed by i) the terms involving only the first derivatives, $\boldsymbol{F}^{\pm}_{H_{DB_{11}}}$, and ii) the second derivatives, $\boldsymbol{F}^{\pm}_{H_{DB_{12}}}$. The terms with second derivatives are expressed as a function of first derivatives using the Green formulation. The force is then expressed as

$$
\begin{aligned}
\boldsymbol{F}^{\pm}_{H_{DB_1}} =& \boldsymbol{F}^{\pm}_{H_{DB_{11}}} + \boldsymbol{F}^{\pm}_{H_{DB_{12}}} \qquad (13)\\
\boldsymbol{F}^{\pm}_{H_{DB_{11}}} =& i\omega^{\pm}\rho \iint_{S_{B_0}} \left(\partial_{\boldsymbol{n}} \Phi_I^{(2)\pm} - \frac{1}{2} \left[\begin{array}{l} \left(\dot{\boldsymbol{\mathcal{X}}}_1^{(1)} - \nabla\Phi_1^{(1)}\right)\cdot R_2^{(1)\mathcal{C}_\pm}(\boldsymbol{n}_0) \\ +\left(\dot{\boldsymbol{\mathcal{X}}}_2^{(1)\mathcal{C}_\pm} - \nabla\Phi_2^{(1)\mathcal{C}_\pm}\right)\cdot R_1^{(1)}(\boldsymbol{n}_0) \end{array} \right]_{S_{B_0}} \right) \boldsymbol{\psi}^{\pm} dS \\
\boldsymbol{F}^{(2)\pm}_{H_{DB_{12}}} =& \frac{i\omega^{\pm}\rho}{2} \iint_{S_{B_0}} \left[\begin{array}{l} \left(\nabla\Phi_2^{(1)\mathcal{C}_\pm}\cdot\nabla\right)\left(\boldsymbol{\psi}^{\pm}\boldsymbol{\mathcal{X}}_1^{(1)}\right) + \left(\nabla\Phi_1^{(1)}\cdot\nabla\right)\left(\boldsymbol{\psi}^{\pm}\boldsymbol{\mathcal{X}}_2^{(1)\mathcal{C}_\pm}\right) \\ -\left(\nabla\cdot\left(\boldsymbol{\psi}^{\pm}\boldsymbol{\mathcal{X}}_1^{(1)}\right)\right)\nabla\Phi_2^{(1)\mathcal{C}_\pm} - \left(\nabla\cdot\left(\boldsymbol{\psi}^{\pm}\boldsymbol{\mathcal{X}}_2^{(1)\mathcal{C}_\pm}\right)\right)\nabla\Phi_1^{(1)} \end{array} \right]\cdot\boldsymbol{n}_0 \; dS \\
& - \frac{i\omega^{\pm}\rho}{2}\int_{\Gamma_0} \left[\left(\boldsymbol{\psi}^{\pm}\boldsymbol{\mathcal{X}}_1^{(1)}\right)\times\nabla\Phi_2^{(1)\mathcal{C}_\pm} + \left(\boldsymbol{\psi}^{\pm}\boldsymbol{\mathcal{X}}_2^{(1)\mathcal{C}_\pm}\right)\times\nabla\Phi_1^{(1)} \right]\cdot d\boldsymbol{\Gamma}.
\end{aligned}
$$

where the segmented water-line, $d\boldsymbol{\Gamma} = (n_{0_2}, -n_{0_1}, 0)d\Gamma$.

The diffraction force due to the free-surface forcing over the finite domain S_{F_1}, $\boldsymbol{F}^{(2)\pm}_{H_{DF_1}}$, is calculated with the evaluated integrands on a user-input free-surface mesh with a circular boundary at radius $r = R_e$. The force is also composed by the terms in first derivatives, $\boldsymbol{F}^{\pm}_{H_{DF_{11}}}$, and second derivatives, $\boldsymbol{F}^{\pm}_{H_{DF_{11}}}$. The second derivative terms are expressed with $\partial_z^2\Phi_I = k^2\Phi_I$ and $\partial_z^2\Phi_P \approx k^2\Phi_P$. The force is then expressed as

$$
\begin{aligned}
\boldsymbol{F}^{\pm}_{H_{DF_1}} &= \boldsymbol{F}^{\pm}_{H_{DF_{11}}} + \boldsymbol{F}^{\pm}_{H_{DF_{12}}}, \qquad (14)\\
\boldsymbol{F}^{\pm}_{H_{DF_{11}}} &= \frac{i\omega^{\pm}\rho}{g} \iint_{S_{F_1}} \left[\begin{array}{l} i\left(\omega_1 \pm \omega_2\right)\left[\nabla\Phi_1^{(1)}\cdot\nabla\Phi_{P_2}^{(1)\mathcal{C}_\pm} + \nabla\Phi_{P_1}^{(1)}\cdot\nabla\Phi_{I_2}^{(1)\mathcal{C}_\pm}\right] \\ -\frac{i\omega_1}{2g}\left[\Phi_1^{(1)}(-\omega_2^2\partial_z\Phi_{P_2}^{(1)\mathcal{C}_\pm}) + \Phi_{P_1}^{(1)}(-\omega_2^2\partial_z\Phi_{I_2}^{(1)\mathcal{C}_\pm})\right] \\ \mp\frac{i\omega_2}{2g}\left[\Phi_2^{(1)\mathcal{C}_\pm}(-\omega_1^2\partial_z\Phi_{P_1}^{(1)}) + \Phi_{P_2}^{(1)\mathcal{C}_\pm}(-\omega_1^2\partial_z\Phi_{I_1}^{(1)})\right] \end{array} \right]_{z=0} \boldsymbol{\psi}^{\pm} dS \\
\boldsymbol{F}^{(2)\pm}_{H_{DF_{12}}} &= \frac{i\omega^{\pm}\rho}{2g} \iint_{S_{F_1}} \left[\begin{array}{l} -\left(i\omega_1\Phi_1^{(1)}\right)k_2^2\Phi_{P_2}^{(1)\mathcal{C}_\pm} - \left(i\omega_1\Phi_{P_1}^{(1)}\right)k_2^2\Phi_{I_2}^{(1)\mathcal{C}_\pm} \\ \mp\left(i\omega_2\Phi_2^{(1)\mathcal{C}_\pm}\right)k_1^2\Phi_{P_1}^{(1)} \mp \left(i\omega_2\Phi_{P_2}^{(1)\mathcal{C}_\pm}\right)k_1^2\Phi_{I_1}^{(1)} \end{array} \right] \boldsymbol{\psi}^{\pm} dS.
\end{aligned}
$$

The diffraction force due to the free-surface forcing over the infinite domain $S_{F_2}, r \in [R_e, \infty]$, $\boldsymbol{F}^{\pm}_{H_{DF_2}}$, is solved semi-analytically. The perturbed and incident potentials are expressed in asymptotic form on a cylindrical coordinate system (r, ϑ, z). The incident potential at $z = 0$ is expressed as

$$
\Phi_{I_j}(r,\nu) = \frac{-ia_j g}{\omega_j}\sum_{l=0}^{\infty}\varepsilon_l i^l J_l(k_j r)\cos l\left(\vartheta - \beta_j\right) \qquad (15)
$$

where $j = 1, 2$ related with the wavenumber k_j, wave frequency ω_j and wave direction β_j, $\vartheta = \tan^{-1}(y/x)$, J_l is the first-kind Bessel function order-l and $\varepsilon_0 = 1$, $\varepsilon_l = 2$ for $l \geq 1$.

The perturbed and radiation potentials are in asymptotic form and expressed in the Kochin function, $\mathcal{H}(\vartheta, \sigma, k, D)$. The Kochin function corresponds with source distribution

functions, the six degree of freedom radiation source distribution, $\boldsymbol{\sigma}_R$, the perturbed source distribution, $\sigma_P(\omega,\beta)$=$\sigma_D(\omega,\beta) - i\omega\boldsymbol{\xi}(\omega)\cdot\boldsymbol{\sigma}_R(\omega)$, that are obtained from the solution of the first order boundary element solver. The Kochin function is defined as

$$\begin{aligned}
\mathcal{H}(\vartheta,\sigma,k,D) &= \sum_{l=0}^{\infty} C_H(\sigma,k,D,l)\cos l\vartheta + S_H(\sigma,k,D,l)\sin l\vartheta \\
C_H(\sigma,k,D,l) &= \frac{-1}{4\pi}\iint_{S_{B0}} \sigma\left(\boldsymbol{x}',\Omega(k,D)\right)\mathcal{Z}(k,D,z')\,\varepsilon_l\,(-i)^l J_l(kr')\,\cos l\alpha' dS \\
S_H(\sigma,k,D,l) &= \frac{-1}{4\pi}\iint_{S_{B0}} \sigma\left(\boldsymbol{x}',\Omega(k,D)\right)\mathcal{Z}(k,D,z')\,\varepsilon_l\,(-i)^l J_l(kr')\,\sin l\alpha' dS
\end{aligned} \tag{16}$$

where $r' = \sqrt{x'^2+y'^2}$, $\alpha' = \tan^{-1}(y'/x')$ on the body panels. Then the radiation and perturbed potentials are expressed, with the Kochin function given in Eq. (16), as

$$\begin{aligned}
\boldsymbol{\psi}_R^{\pm} &= \frac{\sqrt{8\pi k^{\pm}}}{\sqrt{r}}\mathcal{F}(k^{\pm},D,z)e^{i(k^{\pm}r+\pi/4)}\mathcal{H}\left(\vartheta,\boldsymbol{\sigma}_R\left(\boldsymbol{x}',\Omega(k^{\pm},D)\right),k^{\pm},D\right) \\
\Phi_{P_j} &= \frac{\sqrt{8\pi k_j}}{\sqrt{r}}\frac{\mathcal{Z}(k_j,D,z)e^{i(k_j r+\pi/4)}}{k_jD(1-\tanh^2 k_jD)+\tanh k_jD}\mathcal{H}\left(\vartheta,\sigma_P\left(\boldsymbol{x}',\Omega(k_j,D),\beta_j\right),k_j,D\right)
\end{aligned} \tag{17}$$

where the vertical profile $\mathcal{F}(k,D,z) = \frac{\mathcal{Z}(k,D,z)}{kD(1-\tanh^2 kD)+\tanh kD}$. Note that $k^{\pm} = \Omega^{-1}(\omega^{\pm},D)$ is obtained from the dispersion relation.

The diffraction force due to the free-surface forcing over the infinite domain is given as

$$\boldsymbol{F}^{\pm}_{H_{DF_2}} = \frac{i\omega^{\pm}\rho}{g}\left(\mathcal{K}_1^{\pm}(k_1,k_2,\omega_1,\omega_2)\left[\boldsymbol{I}^{\pm}_{DF_{11}}+\boldsymbol{I}^{\pm}_{DF_{12}}\right]+\mathcal{K}_2^{\pm}(k_1,k_2,\omega_1,\omega_2)\left[\boldsymbol{I}^{\pm}_{DF_{21}}+\boldsymbol{I}^{\pm}_{DF_{22}}\right]\right) \tag{18}$$

where

$$\begin{aligned}
&\mathcal{K}_1^{\pm}(k_1,k_2,\omega_1,\omega_2) = \mp i\omega^{\pm}k_1k_2 \\
&\mathcal{K}_2^{\pm}(k_1,k_2,\omega_1,\omega_2) = i\omega^{\pm}\frac{\Omega^2(k_1,D)}{g}\frac{\Omega^2(k_2,D)}{g} \mp \frac{i\omega_1\omega_2}{2}\left(\frac{k_1^2}{\omega_1\cosh^2(k_1D)} \pm \frac{k_2^2}{\omega_2\cosh^2(k_2D)}\right) \\
&\boldsymbol{I}^{\pm}_{DF_{11}} = \int_0^{2\pi}\int_{R_e}^{\infty}\cos(\vartheta-\beta_1)\Phi^{(1)}_{I_1}\Phi^{(1)\mathcal{C}_{\pm}}_{P_2}\,\boldsymbol{\psi}^{\pm}rdrd\vartheta \\
&\boldsymbol{I}^{\pm}_{DF_{12}} = \int_0^{2\pi}\int_{R_e}^{\infty}\cos(\vartheta-\beta_2)\Phi^{(1)}_{P_1}\Phi^{(1)\mathcal{C}_{\pm}}_{I_2}\,\boldsymbol{\psi}^{\pm}rdrd\vartheta \\
&\boldsymbol{I}^{\pm}_{DF_{21}} = \int_0^{2\pi}\int_{R_e}^{\infty}\Phi^{(1)}_{I_1}\Phi^{(1)\mathcal{C}_{\pm}}_{P_2}\,\boldsymbol{\psi}^{\pm}rdrd\vartheta,\ \boldsymbol{I}^{\pm}_{DF_{22}} = \int_0^{2\pi}\int_{R_e}^{\infty}\Phi^{(1)}_{P_1}\Phi^{(1)\mathcal{C}_{\pm}}_{I_2}\,\boldsymbol{\psi}^{\pm}rdrd\vartheta.
\end{aligned}$$

with the potentials defined in Eqs. (15,17). The integral over ϑ can be obtained analytically. The integral over $r\in[R_e,\infty]$ is computed analytically for $r\in[0,\infty]$ subtracted by the numerical integration for $r\in[0,R_e]$.

V – Results

In this section, we show computation results of the QTFs for two classical shapes FOWT concepts platforms; the spar-buoy type platform, SOFTWIND [5] and OC4-semisubmersible platform [11].

Dimension of the platforms are given as follows. The SOFTWIND platform has draft 91.4 m, radius 5.6 m on upper part and 9 m on bottom part. The center of gravity located at (0,0,-71.56) m. The OC4 platform is configured with a main column, radius 3.25 m, draft 20 m, the three columns with heave-plates, the upper columns with radius 6 m, draft 20 m, the base columns with radius 12 m, draft 6 m. The center of gravity is considered at (0,0,0) m.

The floating platforms are discretized in quadrilateral panels using the open-source mesh generator, GMSH [4], as shown in Fig. 1. The SOFTWIND platform is discretized by 1872 panels and the OC4 by 2196 panels. For the sum-frequency QTF computation, the free-surface integral terms are computed on unstructured mesh with 8304 quadrilateral panels over radius 50 m, see Fig. 1. The convergence study of the first order hydrodynamic coefficients are conducted and compared for different number of meshes.

For both floating platforms, the difference-frequencies QTFs (without the free-surface integrals) of surge, heave and pitch are computed with bi-chromatic, bi-directional waves, $\beta_1 = 0°$, $\beta_2 = 30°$, ω_1 and ω_2 in the interval $[2\pi/100, \pi]$ rad/s with the radial frequency step $2\pi/100$ rad/s. The sum-frequency full QTFs, including the free-surface integrals, are computed for the SOFTWIND platform with bi-chromatic waves, $\beta_1 = \beta_2 = 0°$, ω_1 and ω_2 in the interval $[2\pi/100, 2]$ rad/s. In most of the application the free surface terms are negligible in the difference-frequency QTF, but important for the sum-frequency QTF.

The computed results of NEMOH are compared with the results that are obtained using the commercial software, HYDROSTAR. The same mesh is used in both softwares. The lid panels are applied in NEMOH for removing irregular-frequencies with the extended boundary integral method. In HYDROSTAR, similar irregular frequency removal method is applied with the software generated water-plane. Note that, both softwares use difference the green-function model and difference approach for the semi-infinite free-surface integrals.

Next subsections describe the QTFs results. All the QTFs results are nomalized by ρg, where $\rho = 1025kg/m^3$ and $g = 9.81m/s^2$.

V − 1 Difference-frequency QTFs

Comparisons of the normalized magnitude of difference-frequency QTFs, $|\boldsymbol{T}_F^-|/\rho g$ where $\boldsymbol{T}_F^-(0°, 30°, \omega_1, \omega_2) = \boldsymbol{T}_{F_Q}^- + \boldsymbol{T}_{F_P}^-$ and $\boldsymbol{T}_{F_P}^- \approx \left[\boldsymbol{F}_{H_{I_1}}^{\pm} + \boldsymbol{F}_{H_{DB_1}}^{\pm}\right]/a_1 a_2^{\mathcal{C}_\pm}$, Eqs. (10, 12), between HYDROSTAR and NEMOH are shown in the density plots Fig. 2 for the SOFTWIND platform and in Fig. 4 for the OC4 platform. The difference of the QTF results between HYDROSTAR and NEMOH are quantified by $\left(\frac{|\boldsymbol{T}_F^-|_{HYDROSTAR} - |\boldsymbol{T}_F^-|_{NEMOH}}{\rho g}\right)$. Excellence agreement of the results between both softwares are achieved with quite small difference, $< 10\%$ for all the motion modes, as shown in the plots for surge, heave and pitch. More complex density plot is shown in Fig. 4 due to the complex interaction in the OC4 platform.

Off-diagonal QTFs is usually the most relevant info one is looking for when computing QTFs, especially for the mooring design. Detail comparisons of the corresponding off-diagonal QTFs (real and imaginary parts) between both softwares are shown for the SOFTWIND platform in Fig. 3 and for the OC4 in Fig. 5. For the surge and heave motions, the first off-diagonal QTFs are shown, while for the pitch mode the third off-diagonal shown. The $\Delta\omega$ on the first off-diagonal QTF are at the surge natural frequencies and the third off-diagonal QTF are at the pitch natural frequencies of the OC4 platform. Excellence agreements between both software on the off-diagonal QTFs plot are also

achieved. In the plots, it shown that the radiation effect due to the body displacement are dominant in the frequency in interval $\omega < 0.5$ rad/s, while the excitation effect dominant in the other frequency interval $\omega > 0.5$ rad/s. Studying the off-diagonal difference-frequency QTFs at the natural frequencies of the structure are important for understanding low-frequency response of the floating structure.

This verifies the bi-directional difference-frequency QTF computation within NEMOH in the spar-buoy type, SOFTWIND, platform and a more complex structure as OC4-submersible platform.

V – 2 Sum-frequency QTFs

Comparison of the sum-frequency full QTF, $|\boldsymbol{T}_F^+|/\rho g$, where $\boldsymbol{T}_F^+(0°, 0°, \omega_1, \omega_2) = \boldsymbol{T}_{F_Q}^+ + \boldsymbol{T}_{F_P}^+$, Eqs. (10, 12), between both softwares are shown in the density plots, Fig. 6, and in the off-diagonal line plots, Fig. 7. Good agreement are achieved, although in this case the irregular frequency removal method in NEMOH was switched off due to an issue for the computation of the potential on the free-surface mesh. Improvement in this part of NEMOH implementation will be reported in a later publication.

This verifies the full sum-frequency QTF computation (includes the free surface integral) within NEMOH in the spar-buoy type, SOFTWIND, platform.

VI – Conclusion

NEMOH sofware has been extended with a module to compute the bi-directional difference- and sum- frequencies quadratic transfer functions. This novel extension enables the study of second-order wave loads on a structure in multi-directional waves.

This work take place in the FLOATECH project, with the aim of providing a design tool for floating offshore wind turbine (FOWT). Two classical FOWT geometries, the spar-buoy type, SOFTWIND, platform and OC4-semisubmersible platform, are tested and the verification is done on those two geometries.

The difference-frequency, surge, heave and pitch, QTFs results, with the free-surface integral is negligible, has been shown for the both FOWT platforms. The sum-frequency full QTFs results, including the free-surface integrals, has been shown for the Softwind platform. Verification of the NEMOH's results has been performed against the commercial code HYDROSTAR. Excellence agreements between both softwares are achieved.

NEMOH with the QTF module will be soon released publicly, which will be, to our knowledge, the sole and only open-source software that provides the second-order module.

Acknowledgement

This work was done within the framework of the FLOATECH project. This project has received funding from the European Union's Horizon 2020 research and innovation programme under grant agreement No 101007142.

Références

[1] A. Babarit and G. Delhommeau. Theoretical and numerical aspects of the open source BEM solver NEMOH. In *Proceedings of the 11th European Wave and Tidal Energy Conference*, Sept 2015.

[2] Bureau Veritas. HYDROSTAR Software v8.14, 2020.

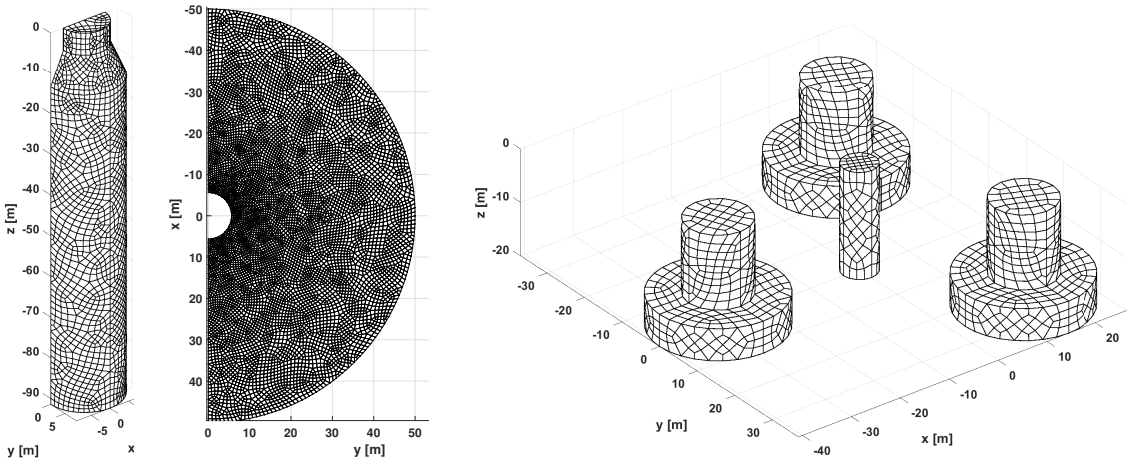

FIGURE 1 – Body boundary mesh and free surface mesh for the SOFTWIND platform, at the left, and body boundary mesh for the OC4-platform, at the right.

[3] X.-B. Chen. *Etudes des réponses du second ordre d'une structure soumise à une houle aléatoire*. PhD Thesis, Université de Nantes, 1988.

[4] C. Geuzaine and J.-F. Remacle. GMSH Software v4.8.4, 2021.

[5] V. Leroy, S. Delacroix, A. Merrien, E. Bachynski-Polić, and J.-C. Gilloteaux. Experimental investigation of the hydro-elastic response of a spar-type floating offshore wind turbine. *Ocean Engineering*, 255 :111430, 2022.

[6] LHEEA, Ecole Centrale Nantes. HOS-Ocean Software, 2022.

[7] B. Molin. Second-order diffraction loads upon three-dimensional bodies. *Applied Ocean Research*, 1(4) :197–202, 1979.

[8] M. Penalba, T. Kelly, and J. V. Ringwood. Using nemoh for modelling wave energy converters : A comparative study with wamit. In *The 12th European Wave and Tidal Energy Conference At Cork, Ireland*, 2017.

[9] M. Philippe, C. P. Adrien Combourieu, F. Robaux, G. Delhommeau, and A. Babarit. Introducing Second Order Low Frequency Loads in the Open-Source Boundary Element Method Code Nemoh. In *Proceedings of the 11th European Wave and Tidal Energy Conference*, Sept 2015.

[10] R. Kurnia, G. Ducrozet, and J.-C. Gilloteaux. Second Order Difference- and Sum-Frequency Wave Loads in the Open-Source Potential Flow Solver NEMOH. In *International Conference on Offshore Mechanics and Arctic Engineering*, volume 5A : Ocean Engineering, 06 2022. V05AT06A019.

[11] A. Robertson, J. Jonkman, M. Masciola, H. Song, A. Goupee, A. Coulling, and C. Luan. Definition of the Semisubmersible Floating System for Phase II of OC4. Technical report, National Renewable Energy Lab. (NREL), Golden, CO (United States), 2014.

[12] P. Schmitt, C. Windt, J. Nicholson, and B. Elsässer. Development and validation of a procedure for numerical vibration analysis of an oscillating wave surge converter. *European Journal of Mechanics - B/Fluids*, 58 :9–19, 2016.

[13] W. Sheng, E. Tapoglou, X. Ma, C. Taylor, R. Dorrell, D. Parsons, and G. Aggidis. Hydrodynamic studies of floating structures : Comparison of wave-structure interaction modelling. *Ocean Engineering*, 249 :110878, 2022.

[14] TU Berlin. QBlade Software, 2022.

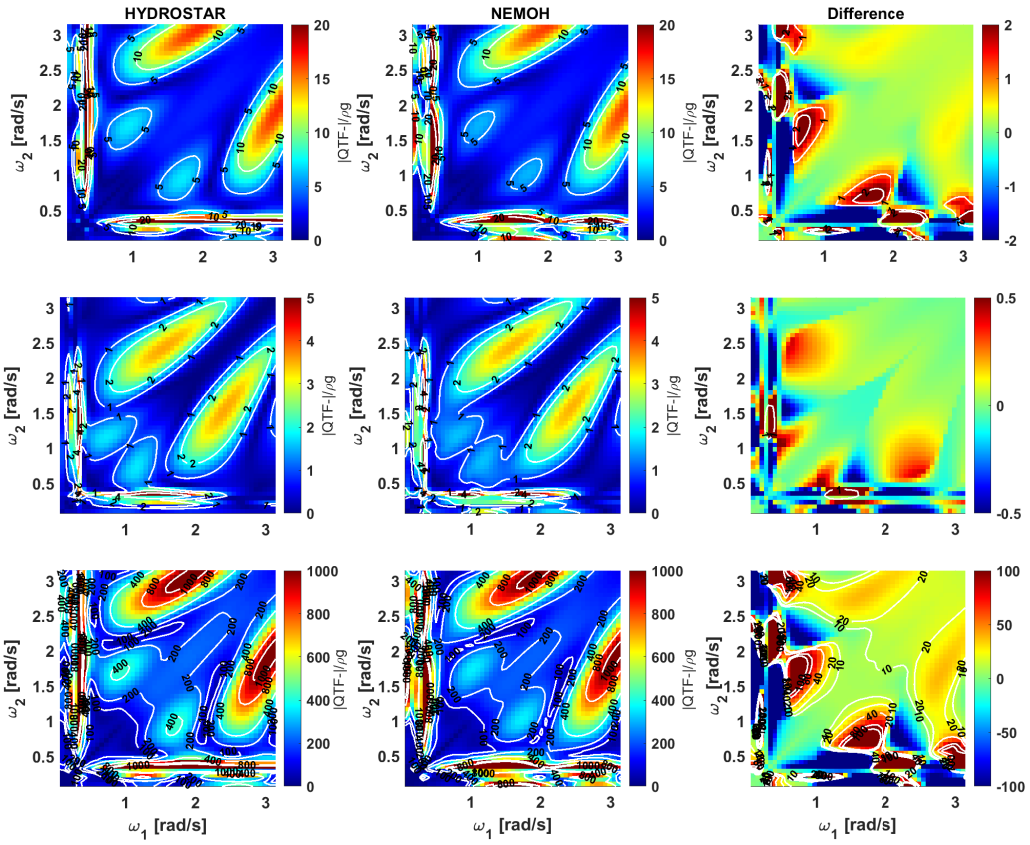

FIGURE 2 – Density plots of the normalized bi-directional surge difference frequency QTF magnitude (without the free-surface integrals) for the floating SOFTWIND platform ; on the top, middle and bottom rows are for surge, heave and pitch, respectively. HYDROSTAR results are on the left column, NEMOH results are on the middle column and the difference on the right column.

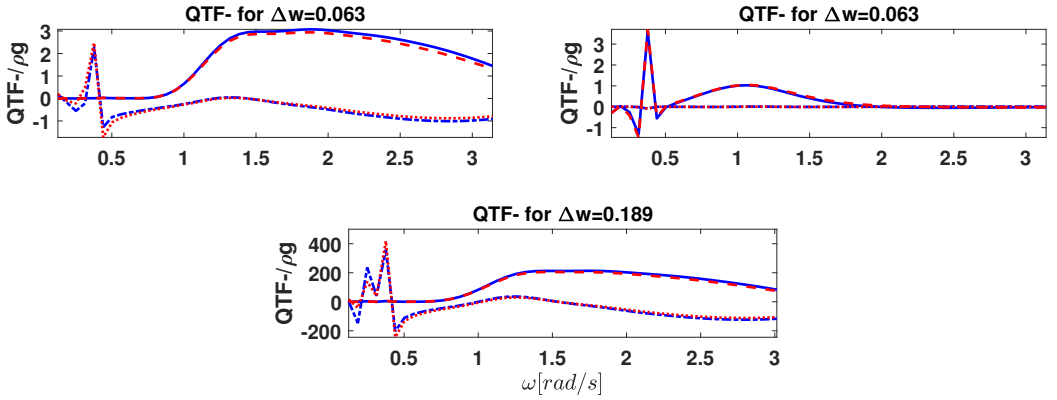

FIGURE 3 – Comparison of the off-diagonal difference frequency QTF for the SOFTWIND platform between HYDROSTAR, real part (blue, solid-line), imaginary part (blue, dashed-dot line) and NEMOH, real part (red, dashed-line), imaginary part (red, dotted-line). On the top-left is for surge, on the top-right for heave (the first off-diagonal) and the bottom for pitch (the third off-diagonal)

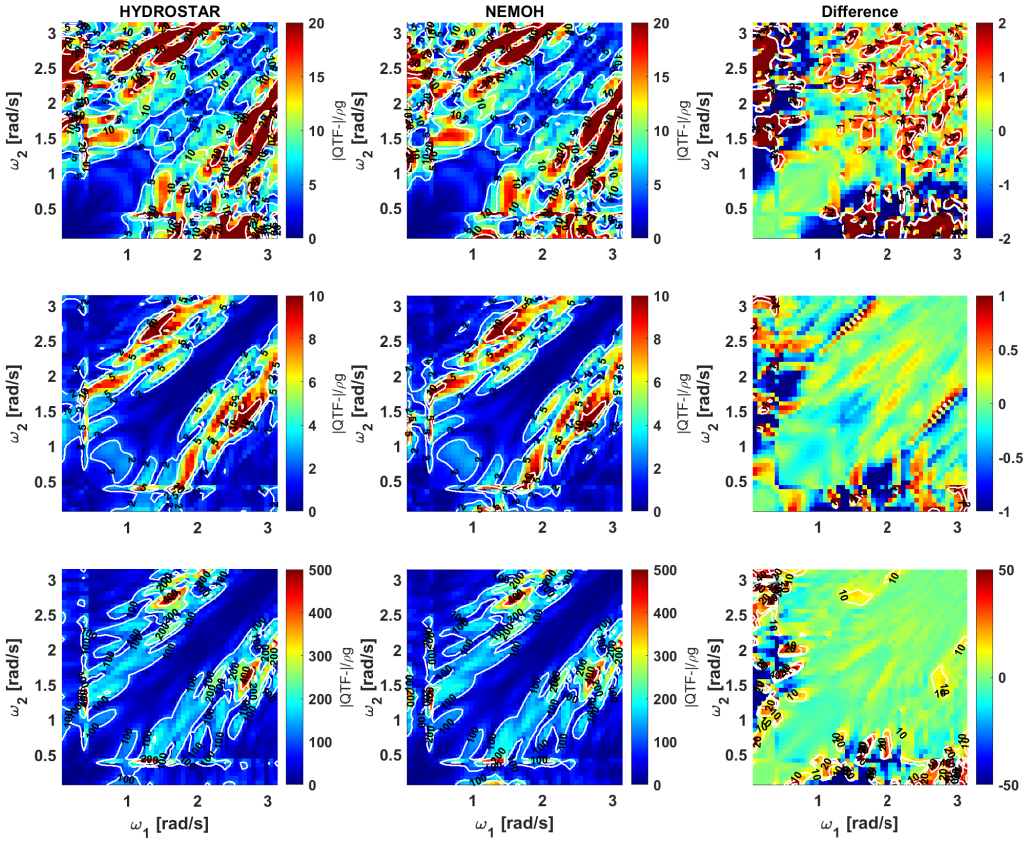

FIGURE 4 – Same description as in Fig. 2 but now for the OC4 platform

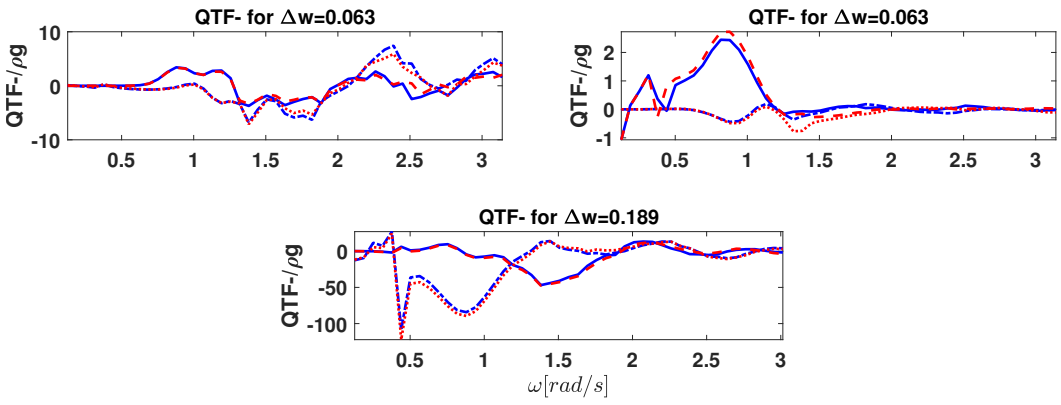

FIGURE 5 – Same description as in Fig. 3 but now for OC4 platform

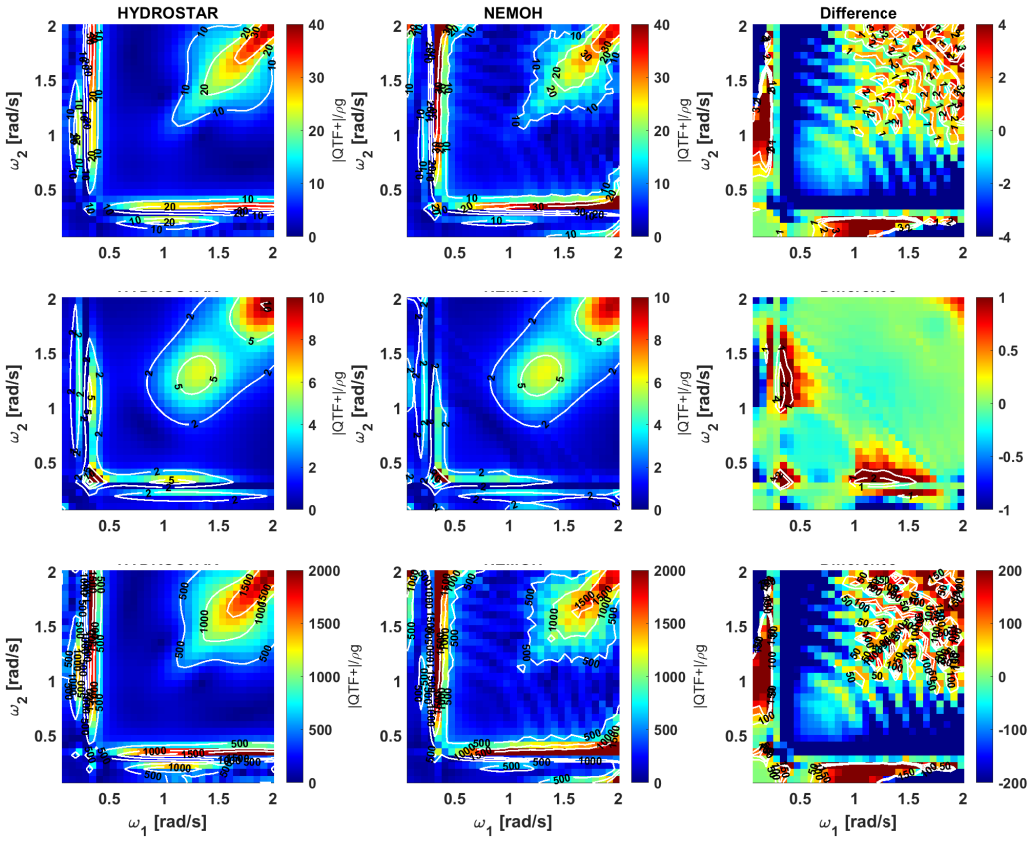

FIGURE 6 – Density plots of the normalized sum-frequency full QTF magnitude (including the free-surface integrals) for the floating SOFTWIND platform ; on the top, middle and bottom row are for surge, heave and pitch, respectively. HYDROSTAR results are on the left column, NEMOH results are on the middle column and the difference in the right column.

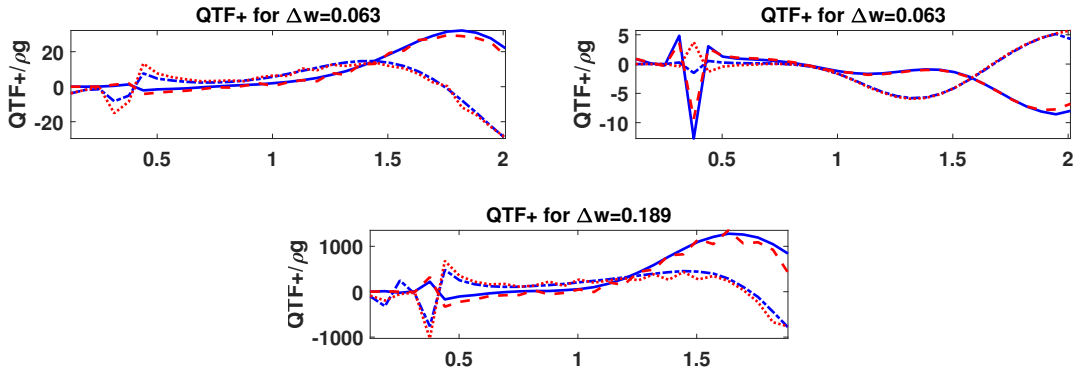

FIGURE 7 – Comparison of the off-diagonal sum-frequency full QTF for SOFTWIND platform between HYDROSTAR, real part (blue, solid-line), imaginary part (blue, dashed-dot line) and NEMOH, real part (red, dashed-line), imaginary part (red, dotted-line). On the top-left is for surge, on the top-right for heave (the first off-diagonal) and the bottom for pitch (the third off-diagonal)